ESTIMATION OF SIMULATION ERRORS IN THE EUROPEAN TRANSONIC WIND TUNNEL (ETW) *

Bernhard Wagner
Theoretical Aerodynamics, Dornier GmbH
Friedrichshafen, F. R. of Germany

Abstract

Simulation errors in cryogenic wind tunnels caused by real gas effects, changes in viscosity and heat conductivity characteristics at low temperatures, heat transfer, and local condensation are estimated theoretically. For this purpose viscous effects and heat transfer influences in transonic high Reynolds number turbulent flows are calculated by solving numerically the full Navier-Stokes equations for shock wave boundary layer interactions and by calculating boundary layers on airfoils, real gas equations of state and non-adiabatic walls being included in both procedures. Equilibrium condensation approximating the case of heterogeneous nucleation is investigated in transonic airfoil flows by means of numerical solutions of the full inviscid Euler equations. The separation behavior is shown not to be sensitive to real gas effects and small amounts of heat transfer. The condensation influence is primarily seen by a considerable drag increase.

I. Introduction

The most promising chance for establishing very high Reynolds number transonic flows in laboratory experiments is through the use of cryogenic wind tunnels. However, by changing to the low temperatures of a cryogenic tunnel and to increased pressures, some deviations from the results at ambient conditions can occur which can be estimated from a theoretical point of view. Such possible differences being treated in the present work for the usual test gas nitrogen are deviations from the behavior of ideal gases, changes in viscosity and heat conductivity characteristics, heat transfer due to not correctly cooled-down model surfaces, and small amounts of condensation after the saturation boundary is crossed. A recent review on the efforts undertaken in the United States and in Europe has been given by Hall (1).

Previous studies (e.g. Adcock et al.(2)) showed the insignificance of thermodynamic real gas effects (without condensation) in pure inviscid flow of cryogenic nitrogen. But small systematic effects in skin friction have been detected in a first trial to calculate a sensitive viscous case under cryogenic conditions, namely a supersonic shock wave laminar boundary layer interaction (3,4). In references 3,4 the explanation was offered that the observed net effect in skin friction results from two opposing effects, firstly from a change of the wall temperature due to real gas effects and secondly from a slight slope change of the viscosity characteristic when going to low temperatures. These conjectures were confirmed by a thoroughly detailed investigation of laminar and turbulent boundary layers in cryogenic nitrogen by Adcock and Johnson (5). On the other hand, Inger (6) suggested on the basis of parametric calculations the possibility of stronger effects in the case of normal shock-turbulent boundary layer interaction, but this possibility was called in question by Adcock (7) in the light of his boundary layer analysis already mentioned (5). Hence, one purpose of the present study was the clarification of these influences upon the transonic shock-turbulent boundary layer interaction by numerical solutions of the full Navier-Stokes equations. The calculations were carried out with the aid of MacCormacks L-U-scheme (8) including an algebraic two layer eddy viscosity turbulence model and a real gas analysis based on the Beattie-Bridgeman equation (9). Of special interest was the shock induced separation under cryogenic conditions. In order to account for the influence of not correctly cooled-down model surfaces, cases with nonadiabatic wall conditions have been also treated. Furthermore, the real gas equations of state were introduced into a non-adiabatic boundary layer method (10) to study similarly the separation behavior on airfoils in transonic cryogenic flow.

In the equilibrium condensation process the pressure as a function of the temperature is assumed to follow the vapor pressure curve after the liquefaction boundary has been reached. Therefore, this case approximates the limit of heterogeneous nucleation where the number of nuclei is sufficiently large to start the condensation immediately after obtaining saturation. Those nuclei can originate in impurities of the test gas or in incompletely evaporated droplets after injection of liquid nitrogen. Heterogeneous nucleation is a pessimistic assumption since usually some amount of supersaturation is observed which causes a favourable lag of condensation onset. However, in order to estimate the basic influence of condensation on the flow field this assumption was introduced into a finite volume method (11) for solving numerically the Euler equations for two-dimensional inviscid flow. In this manner transonic airfoil flows were studied which are known to be particularly sensitive to heat release which is the main effect of condensation. For simplicity ideal gas equations of state were applied for the vapor phase although ref. 12 indicates considerable influence of the real gas equations on condensation. Accordingly, the real gas influence was estimated by calculation of one-dimensional nozzle flow corresponding to the states on a wall streamline of an airfoil for ideal gas flow without condensation.

Ref. 13 contains the details of the present subject

* This research was sponsored by the German Ministry of Research and Technology under support number LVW 7901 and by the Technical Group ETW, Amsterdam under contract ETW/79/01/68730/143963

II. Analysis

Thermodynamic Behavior and Material Properties

The real gas influence on the thermodynamic states is described by the thermal equation of state of Beattie-Bridgeman and a caloric equation of state derived from it by thermodynamic considerations as pointed out in references 3,4. This system of equations contains in addition to the gas constant R five constants, the values for nitrogen and air also being given in ref. 3,4. While all cryogenic examples calculated represent cases of realistic nitrogen flow in a wind tunnel, the ideal gas cases compared correspond to flight conditions at the lower edge of the stratosphere.

Molecular viscosity and heat conductivity are represented separately by the well known Sutherland formula where the two constants for each have been fitted to the available experimental material (3,4). In ideal gas calculations used for comparison the heat conductivity has been computed from the viscosity by means of a constant Prandtl number value of Pr = 0.72.

For the boundary layer method (10) a constant Prandtl number has to be used generally. From the boundary layer equations a real Prandtl number can be derived for real gas boundary layers, which varies across the boundary layer (14). But calculating the variation of this Prandtl number retrospectively from the results achieved with constant Prandtl number and running the boundary layer program additionally with the upper and lower limit values of the variation range, it was shown that the influence of the variation of the real Prandtl number is negligible compared to the sum of all other real gas effects. Hence, it is always sufficient for cryogenic nitrogen to use an average Prandtl number.

Turbulence Model

The turbulence model used is the algebraic model of Cebeci and Smith (10), a two layer eddy viscosity model. Such a relatively simple model is used exclusively since numerical experiments with different turbulence models in shock wave-boundary layer calculations did not show convincing advantages of the higher order models (15). No special account can be given for the cryogenic conditions since no information is available on the turbulent behavior of a real gas at low temperature. Therefore, the eddy heat conductivity k_t is calculated from the eddy viscosity and the constant turbulent Prandtl number $Pr_t = 0.9$ by using the ideal value of the specific heat at constant pressure c_{pid}

$$k_t = c_{pid}\, \varepsilon_t / Pr_t .$$

Equilibrium Condensation

The key for equilibrium condensation investigations is the postulate that once the vapor pressure curve is reached during an expansion, the pressure p does not further depend on density but only on temperature T. Therefore, the total differential of p yields for the mixture of vapor and condensate

$$\frac{dp}{dT} = \left(\frac{\partial p}{\partial T}\right)_{\varrho} = \frac{dp_v}{dT} \qquad (1)$$

where $p_v(T)$ represents the vapor pressure curve. By demanding the mixed second order derivatives of the free energy to be equal the following relation is established (see e.g. ref. 16)

$$\left(\frac{\partial p}{\partial T}\right)_{\varrho} = \left(\frac{\partial s}{\partial v}\right)_T \qquad (2)$$

with s being the specific entropy and $v = 1/\varrho$ the specific volume. The latent heat L is by definition the difference between the enthalpies h of vapor and condensate phases at constant temperature which can also be expressed by the entropy difference

$$L = h_v - h_c = T\,(s_v - s_c) \qquad (3)$$

where the subscripts v and c refer to the vapor and condensate phases, respectively. For the mixture all extensive state variables are given by linear relations, e.g.

$$v = v_v\,(1-g) + v_c g = v_v + g\,(v_c - v_v), \qquad (4)$$

$$h = h_v(1-g) + h_c g = h_v + g\,(h_c - h_v) = h_v - gL \qquad (5)$$

with g denoting the condensed mass divided by the whole mass of vapor and condensate. Hence, a combination of Eqs. (1) and (5) results in

$$\frac{dp}{dT} = \frac{1}{T}\,\frac{h_v - h_c}{v_v - v_c} = \frac{L}{T}\,\frac{1}{v_v - v_c} \qquad (6)$$

representing the Clausius-Clapeyron equation.

If the thermodynamic state is sufficiently far away from the critical point, the condensed volume v_c can be neglected and the latent heat is approximately constant. Then, Eq. (6) yields after introducing the thermal equation of state for the pure vapor and integrating

$$p_v(T) = \alpha \cdot e^{-\beta/T}. \qquad (7)$$

This approximation of the vapor pressure proves to be always very good, although the latent heat is not exactly constant. Fitting the constants α and β to the nitrogen table data (17) gives the values

$$\alpha = 8705 \text{ bar} \; ; \; \beta = 701.7 \text{ K}$$

for liquid condensate which is mainly of importance for cryogenic wind tunnels. Recalculating the latent heat L from Eq. (7) by means of Eq. (6) and neglecting v_c, L is approximated by

$$L = \frac{1}{\varrho_v}\,\frac{\beta}{T}\,p_v(T)$$

which reduces by use of the thermal equation of state to a constant in the case of ideal gas behavior of the vapor

$$L = R\beta \; . \qquad (8)$$

Neglecting v_c also in Eq. (4) results in

$$\varrho_v = \varrho(1-g) \qquad (9)$$

and the thermal equation of state for the mixture can be derived from that of the vapor

$$p = \varrho\,(1-g)\,RT. \qquad (10)$$

Using Eqs. (5), (6) neglecting v_c, and (9), the first law of thermodynamics reads as

$$dh - dp/\varrho = dh_v - d(gL) - L(1-g)\, dT/T = 0. \qquad (11)$$

For ideal gas, L is a constant (see Eq. (8) and h_v is proportional to the temperature by the factor C_p Then, Eq. (11) can be integrated leading to

$$g = \frac{h_v}{L} \ell n \frac{h_v}{h_{v_s}} + 1 - \frac{h_v}{h_{v_s}} \qquad (12)$$

where h_{v_s} is the saturation vapor enthalpy indicating the point of the vapor pressure curve for which saturation is reached first. This closed expression for the condensed mass fraction g (12) was originally shown by Buhler (18); it is derived here by pure thermodynamic arguments without referring to the flow equations and is, therefore, valid for an entire two- or three-dimensional flow field, provided the flow is homentropic (i.e.: constant h_{v_s} in the whole field). Since Eq. (12) can be used to eliminate g from Eqs. (5) and (10), these equations together with the proportionality relation mentioned for h_v form a set which replaces appropriately the ideal gas equations of state after the liquefaction boundary is crossed.

Flow Equations and Numerical Methods

For calculating the flow field for shock-boundary layer interaction on a flat plate the full time-dependent Navier-Stokes equations are solved numerically. The numerical method used is the "L-U-scheme" of MacCormack (8) which is second order accurate in space and time. In contrast to the older explicit scheme (used in references 3,4) it contains an implicit step and is thus unconditionally stable. Therefore, the method is appropriate for the economical computation of high Reynolds number flows, and in the present study Reynolds numbers up to 20 millions (based on the distance between leading edge and shock position) are verified with local Courant numbers up to 1000 in regions close to the wall. In essence, it represents a finite volume method that is well suited for the inclusion of real gas equations of state (see e.g. ref. 3,4). The mesh is rectangular and contains 32 x 32 mesh points. For a good resolution of the physical phenomena the mesh exhibits a dense spacing close to the wall in the normal direction following an exponential law and a coarse one outside of the boundary layer. Also in the direction parallel to the plate a stretching is necessary to allow a fine spacing in the interaction region. After a converged solution is achieved in the original mesh, the discretisation is refined by halving the longitudinal intervals in the interaction region. By a repetition of the calculation procedure the final solution is found. Arbitrarily, adiabatic or nonadiabatic boundary conditions can be prescribed at the wall. For the nonadiabatic cases a constant wall temperature is chosen being a definite amount above the mean value of the recovery temperatures upstream and downstream of the shock.

The boundary layer code used for boundary layer calculations on airfoils is a well known finite difference method (10). It allows for nonadiabatic walls by prescribing wall temperature or heat flux and for the inclusion of arbitrary real gas equations of state, but basically a constant Prandtl number is postulated. As already mentioned, the real variations of the Prandtl number could be shown to be negligible in the present case. For simulating nonadiabatic cases a constant wall temperature was chosen being a definite amount above the total temperature of the approaching flow.

In the condensation calculations consideration of different dynamic behaviors of droplets and vapor is necessary since the velocity differences between vapor and droplets are negligible for the small droplet sizes being found in such flows (19). The time dependent form of the conservation laws for mass and momentum reads in vector form as (t = time)

$$\frac{D\varrho}{Dt} + \varrho \,\mathrm{div}\, \vec{V} = 0, \qquad (13)$$

$$\varrho \frac{D\vec{V}}{Dt} + \mathrm{grad}\, p = 0 \qquad (14)$$

where the density ϱ represents the mean value for the mixture of vapor and condensate (20). The conservation of energy can be written for flow regions where condensation is present (20).

$$\frac{D}{Dt}\left(\frac{V^2}{2} + h_v - gL \right) - \frac{1}{\varrho} \frac{\partial p}{\partial t} = 0.$$

If only the converged steady state is of interest the stationary form of the energy equation can be used exclusively, leading to a simplified calculation and to accelerated convergence (11). Hence, the energy equation is simplified to

$$\frac{V^2}{2} + h_v - gL = \text{const.} = h_{t_\infty} \qquad (15)$$

with h_{t_∞} being the total enthalpy of the approaching uncondensed flow. Applying the three equation finite volume method for solving the Euler equations (13) and (14) in an integral form, ϱ and V result immediately from equations (13) and (14). Hence, combining Eqs. (15) and (12) the vapor enthalpy h_v can be calculated iteratively

$$h_{v,i+1} = \frac{h_t - \frac{V^2}{2} + L}{1 + \frac{L}{h_{v_s}} - \ell n \frac{h_{v,i}}{h_{v_s}}} \qquad (16)$$

and from Eqs. (10) and (12) follows p via computation of temperature T from h_v. Carrying out only one iteration of Eq. (16) at one time step the procedure becomes very economic since for the converged flow field the solution of Eq. (16) is converged, too. Afterwards the condensed mass fraction is found from Eq. (12) and the pressure follows from Eq. (10) introducing directly hv instead of T (ideal gas).

$$p = \varrho\,(1-g)\,\frac{\gamma - 1}{\gamma}\, h_v. \qquad (17)$$

Proceeding to a dimensionless form $\bar{p}, \bar{\varrho}$, pressure p and density ϱ are divided by their undisturbed upstream values p_∞ and ϱ_∞, respectively. If the form of Eq. (17) is to be retained in dimensionless variables for consistency with usual thermodynamic formulas, the dimensionless enthalpy $\bar{h_v}$ must be defined with the aid of the enthalpy of the undisturbed flow

$$\bar{h}_v = \frac{\gamma}{\gamma-1}\,\frac{h_v}{h_\infty} \quad . \tag{18}$$

Introducing Eq. (18) into Eq. (12) the following similarity parameter turns out for condensing flows

$$\bar{L} = \frac{\gamma}{\gamma-1}\,\frac{L}{h_\infty} \quad . \tag{19}$$

Besides fixing this parameter it must be specified for an actual flow at which value of the enthalpy h_{v_s} the computation is to be switched from ideal gas equations of state for pure vapor to the wet vapor equations presented above. Since the definition of a constant value h_{v_s} makes only sense in an isentropic flow, the prescription of a saturation Mach number M_s is sufficient for which the vapor pressure is just reached. While M_s, being the most interesting parameter, is varied for the different sample calculations of the present study, the value of the dimensionless latent heat $\bar{L}$ (19) is adjusted to actual states in the ETW which correspond to the highest stagnation pressure of 4.5 bar. Nevertheless, $\bar{L}$ changes slowly with the actual conditions indicating the calculations to be exemplary for other cryogenic wind tunnels, too. Errors in the assumed constancy of h_{v_s} occur when shock waves are crossed before the condensate is completely re-evaporated. But the resulting jumps in h_{v_s} appear to remain small in the transonic flow regime because of the weakness of the shock waves.

For estimating the real gas influence on the equilibrium condensation process a finite difference procedure has been established including the one-dimensional flow equations and all thermodynamic relations in differential form. The integration is carried out applying a simple iterative predictor-corrector method and using a given stream tube area ratio which corresponds to the velocity distribution on a wall streamline of an airfoil in ideal gas flow.

III. Results

Shock-Boundary Layer Interaction

Fig. 1 presents the calculated distributions of wall pressure p_w and skin friction coefficient c_f versus local Reynolds number for a nonadiabatic case. The wall temperature is assumed to be 10 percent higher than the adiabatic mean recovery temperature. The shock position is fixed by the boundary conditions applied at the outer boundary of the computational domain extending about 10 times the boundary layer thickness. The Reynolds number based on the longitudinal distance of this position from the leading edge amounts to 20 million. The boundary layer is assumed to start turbulently at the leading edge. Since no difference can be seen between adiabatic and isothermal wall results within the plot accuracy, these deviations are additionally presented in a larger scale. The deviation for the wall pressures p_w is negligible except that the peak at the beginning of the interaction indicates a slight upstream shift of interaction start while the following steep pressure ascent appears to be a little flattened. The extension and the form of the separation bubble shown in the skin friction plot are not noticeably affected although a systematic reduction of the skin friction coefficient c_f is evident upstream and downstream of the interaction region. The effects on p_w/p_∞ and c_f correspond to the known trends for nonadiabatic walls, but a substantial shift of separation onset suspected by Inger (6) is not found for small temperature differences.

Fig. 2 shows the corresponding plots for a typical cryogenic nitrogen flow where the undisturbed state upstream of interaction is related to a point on the vapor pressure curve for 4.5 bar stagnation pressure since the largest real gas effects can be expected close to saturation. Again no deviations can be detected in the usual plot scale. But looking at the differences in the ratio of wall pressure to undisturbed pressure, a small deviation can be seen being almost totally within the numerical scatter upstream of the shock while it approaches to the difference in the inviscid external flow downstream of the shock due to the real gas influence on the shock wave when the upstream Mach number is fixed. This observation agrees with the impression of the external pressure onto the boundary layer suggested by boundary layer theory. Only at the beginning of the interaction the pressure difference exhibits a pronounced negative peak pointing out a little downstream shift of the interaction similar to the expectations for a cooled wall. The skin friction values downstream of the shock are of the estimated order of magnitude (see reference 4), while the upstream c_f shows an unexpected variation apparently due to numerical errors in consequence of different numerical treatment of the equations of state (pointed out in ref. 3,4). Besides the positive peak at the beginning of the interaction already explained above by a slight shift, definitely no influence on the separation bubble can be seen. Hence, a sensitivity to real gas effects as suggested by Inger (6) is not observed. An explanation for the downstream shift of the beginning of interaction can be drawn from Fig. 3 where the corresponding temperature distributions are depicted for a number of longitudinal stations. The Reynolds number Re_y based on the distance normal to the wall ranges in Fig. 3 over one tenth of the boundary layer thickness. The ratio of the local temperature to the static temperature of the undisturbed flow is for real cryogenic nitrogen always less than that for ideal air at ambient temperature. This fact results in a slightly thinner boundary layer for real nitrogen leading to a reduced upstream influence of the interaction.

Fig. 4 contains a case for which only the static temperature of the undisturbed flow is lowered by about 10 K compared with the case of Fig. 2. This situation corresponds to an approaching flow which has considerably penetrated the supersaturated region beyond the liquefaction boundary. Without accounting for condensation, this example is chosen in order to estimate for the first time how a flow behaves in that region which is hoped to be reached by taking advantage of the favourable effect of condensation delay due to homogeneous nucleation (1). This calculation is, of course, somewhat speculative since it is presently not known whether the thermodynamic states actually follow the extrapolation by the equations of state used here beyond the vapor pressure curve. Nevertheless, the results presented in Fig. 4 show very small deviations, too. Only a small additional

effect occurs in c_f at the end of the bubble indicating a slightly earlier reattachment which could also be exaggerated by numerical sensitivity.

Boundary Layer Calculations

An example of the boundary layer calculations performed is shown in Fig. 5. It is based on the velocity distribution of an Euler solution (see equilibrium calculations) for the Dornier supercritical airfoil Do A2 (identical with CAST 10). Transition is assumed to occur at a Reynolds number of about 3 million. The skin friction coefficient c_f is plotted versus local Reynolds number based on the arc length on the profile surface measured from the stagnation point. The overall Reynolds number based on the chord length is 50 million.

Differences due to real gas effects can not be detected in the normal scale of the figure. But also in the rather enlarged scale for the difference between real and ideal gas the deviations are extremely small ranging far below the limit of one drag count (contribution of 10^{-4} to the drag)and guaranteeing therefore from this point of view an extremely good accuracy for the measurements in the planned ETW. The situation is especially favourable for the ETW since the designed maximum stagnation pressure of 4.5 bar is close to the region of lowest real gas influences for viscous flow as clearly stated in previous investigations (5). In this region the effect of different temperature distribution being seen in Fig. 3 cancels almost exactly the effect of a steeper slope of the viscosity characteristic in the low temperature range. The separation behavior is not visibly affected by real gas effects, neither on the upper surface where the separation is caused by the shock nor on the lower surface where separation occurs only very close to the trailing edge.

The nonadiabatic case also shown in Fig. 5 is characterized by an isothermal wall having a wall temperature which is 20 percent above the total temperature of the approaching undisturbed flow $T_{t\infty}$. The skin friction coefficient is lowered by an amount which corresponds almost exactly to one drag count. This amount agrees very well with that expected from the Navier-Stokes solutions calculated with the temperature difference being about a half of the present case (Fig. 1). These results correspond also to a previous study of Green, Weeks, and Pugh (21) where the equivalence of a hot wall to a Reynolds number reduction is discussed in detail.

Equilibrium Condensation in Airfoil Flow Fields

Calculations in the transonic flow regime are carried out for two airfoil sections, namely for the NACA 0012 at angle of attack and for a typical supercritical airfoil Dornier A2 (identical with CAST 10). The computational mesh is an O-mesh containing 128 x 33 grid points (128 points on the surface).

In Fig. 6 the results for the NACA 0012 are presented whereby three different saturation Mach numbers M_s are selected with correspondingly adjusted values of $\bar{L}$ while all other parameters remain unchanged. On the left hand side for each case an inner part of the mesh is shown with the supersonic zones and the condensation regions being depicted. The outer part of the mesh is omitted since its stretching in the radial direction would diminish the scale considerably. On the right hand side the corresponding distributions of the pressure coefficient on the upper and lower surfaces are given.

In the first case (Fig. 6a) with $M_s = 1.2$ the saturation boundary is somewhat exceeded on the upper surface (maximum local Mach number 1.3) while condensation on the lower surface (maximum local Mach number 1.2) is still avoided. No visible changes of the supersonic regions and of the pressure coefficient are present although the condensation region above the airfoil exhibits a considerable size. Decreasing the saturation Mach number to $M_s = 1.1$ (Fig. 6b), the upper condensation zone is spread out and also such a zone under the lower surface is established. But the extension of the supersonic zones is only affected by a slight downstream shift of the terminating shocks. The pressure coefficient exhibits small variations in the whole condensation range and shows also clearly the downstream travelling of the shock position. In these cases the condensate completely evaporates immediately upstream of the shocks while in reality the evaporation should coincide with the shock. This small unimportant difference results from the smearing out of the shocks by the shock capturing process of the numerical method.

Finally, a saturation Mach number of $M_s = 0.801$ is chosen which is almost equal to the Mach number of the undisturbed flow $M_\infty = 0.8$ (this small difference being introduced in order to avoid computational difficulties). Hence, the condensation onset precedes now the transition to supersonic flow. Surprisingly, the calculation procedure leads to a converged steady state solution without any additional problem although the high sensitivity of the flow to heat addition when approaching a Mach number of unity is well known (22). The supersonic regions are now (Fig. 6c) considerably but not principally changed in their form. The sonic line at their beginning and the terminating shocks are distinctly shifted downstream and the lateral extension of the supersonic zones is increased. Moderate changes appear in the pressure distribution but again the pronounced downstream shift of the shocks is obvious.

Fig. 7 shows a result for the Do A2 airfoil (CAST 10) with saturation Mach number $M_s = 1.2$ (maximum local Mach number on upper surface being about 1.41). Due to the transonic design for the lifting section, only on the upper side a supersonic region is present extending over a large region and filled out largely by the condensation zone. A reasonable shock terminates the supersonic zone for the present off-design conditions and this shock is again slightly shifted downstream.

The impact of condensation on the lift coeffienct is presented in Fig. 8. It shows the relative shift in the lift coefficient C_L (C_{LC} with condensation; C_{LO} without condensation) versus saturation Mach number. Obviously, the C_L-changes remain small reducing C_L even in the limiting case of free stream saturation ($M_s \approx M_\infty$) only by 2 percent. However, the drag changes tremendeously as Fig. 9

indicates. While all comparisons up to this point state only gradual changes, these results forbid large penetrations into the region of locally condensed flow if substantial drag errors shall be avoided. These results are in accordance with the common knowledge on heat release (22), because heat addition in regions of reduced velocity (e.g. stagnation point) produces thrust while additional drag must be expected for heat release at increased velocity (e.g. maximum thickness of profiles).

Fig. 10 gives an impression how large the condensed mass fraction becomes for $M_s = 1.1$ on the wall streamlines which are the most critical ones. g ranges only up to 2.5 percent and even in the free stream saturation case of Fig. 6c 4 percent is not exceeded.

Finally, Fig. 11 shows the results for recalculating the condensed mass fraction from a one-dimensional computation with prescribed stream tube area corresponding to the ideal gas Mach number distribution in the real two-dimensional airfoil flow. g is plotted versus the real arc length s in cm which is representative for a case of 50 million Reynolds number in the ETW. The dashed line shows the result achieved in the prescribed stream tube combining the condensation relations with ideal gas assumptions. Comparing with the original two-dimensional result (solid line), it becomes obvious that the streamline deviation by condensation in the two-dimensional flow affects g significantly but no principal change occurs. Furthermore, the difference between the dashed-dotted line and the dashed line represents the real gas effect (starting with the same conditions in the approaching undisturbed flow) which was already suggested to have a significant influence on g (12). The effect is considerable but the flow does not change its character.

IV. Conclusions

Concerning viscous effects in adiabatic flows of cryogenic nitrogen the present investigation shows that the separation mechanism appears not to be noticeably changed compared with the case of ideal air at ambient temperatures. This result is found from Navier-Stokes solutions for the transonic shock wave-turbulent boundary layer interaction as well as from boundary layer calculations in transonic flow. The systematic deviation of the skin friction coefficient already detected in previous investigations remains very small in the operating range of the ETW. Also hot walls with temperatures up to about ten percent above the recovery temperature do not essentially affect the separation behavior although their influence on the skin friction is noticeable.
The errors due to the presence of condensation are shown by two-dimensional calculations for equilibrium condensation in transonic flow fields. The results suggest that small amounts of condensation do not visibly influence the measurements. The onset of condensation can be first detected from a significant drag increase. One-dimensional calculations for a stream tube corresponding to an airfoil surface streamline in ideal gas flow without condensation indicate the affects of two-dimensionality and of real gas equations of state on the condensation to be noticeable but not fundamental.

V. References

(1) Hall, R.M.: Real gas effects I - Simulation of ideal gas flow by cryogenic nitrogen and other selected cases. And:Real gas effects II - Influence of condensation on minimum operating temperatures of cryogenic wind tunnels. In: AGARD Lecture Series 111 on "Cryogenic Wind Tunnels", 1980

(2) Adcock, J.B., Kilgore, R.A., and Ray, E.J.: Cryogenic nitrogen as a transonic wind tunnel test gas. AIAA-Paper 75-143, 1975

(3) Wagner, B. and Schmidt, W.: Theoretical investigations of real gas effects in cryogenic wind tunnels. AIAA-Journal, Vol.16, pp. 580-586, 1978

(4) Wagner, B. and Schmidt, W.: Theoretische Untersuchungen zur Stoß-Grenzschicht-Wechselwirkung in kryogenem Stickstoff. Zeitschrift für Flugwissenschaften und Weltraumforschung, Vol. 2, pp. 81-88, 1978

(5) Adcock, J.B. and Johnson, C.B.: A theoretical analysis of simulated transonic boundary layers in cryogenic-nitrogen wind tunnels. NASA Technical Paper 1631, 1980

(6) Inger, G.R.: Transonic shock-boundary-layer interactions in cryogenic wind tunnels. Journal of Aircraft, Vol. 16, pp. 284-287, 1979

(7) Adcock, J.: Simulation of flat-plate turbulent boundary layers in cryogenic tunnels. Journal of Aircraft, Vol. 17, pp.284-285,1980

(8) MacCormack, R.W.: A numerical method for solving the equations of compressible viscous flow. AIAA-Paper 81-0110, 1981

(9) Landolt-Börnstein: Zahlenwerte und Funktionen, IV. Band, 4. Teil, Bandteil a. 6. Auflage (herausgegeben von H. Hausen), Springer-Verlag, Berlin/Heidelberg /New York, 1967

(10) Cebeci, T. and Smith, A.M.O.: Analysis of turbulent boundary layers. Academic Press, New York, 1974

(11) Jameson, A., Schmidt, W., and Turkel, E.: Numerical solutions of the Euler equations by finite volume methods using Runge-Kutta time-stepping schemes. AIAA-Paper 81-1259, 1981

(12) Bursik, J.W. and Hall, R.M.:
Effects of various assumptions on the calculated liquid fraction in isentropic saturated equilibrium expansions.
NASA Technical Paper 1682, 1980

(13) Wagner, B.:
Estimation of Simulation Errors and Investigations on Operating Range Extensions for the European Transonic Windtunnel ETW.
Dornier Report FB 81BF/8B, 1981

(14) Wagner, B.:
Boundary Layer Calculations for Cryogenic Wind Tunnel Flows. To be published in the commorative volume on Thermodynamics and Fluiddynamics dedicated to Prof. A. Walz on the occasion of his 75th birthday, Springer-Verlag, 1982

(15) Viegas, J.R. and Horstman, C.C.:
Comparison of multi-equation turbulence models for several shock boundary layer interaction flows.
AIAA-Journal, Vol. 17, pp. 811-820, 1979

(16) Baehr, H.D.:
Thermodynamik. 2. Auflage, Springer-Verlag, Berlin/Heidelberg/New York, 1966

(17) Jacobsen, R.T. and Stewart, R.B.:
Thermodynamic properties of nitrogen including liquid and vapor phases from 64 K to 2000 K with pressures to 10000 bar.
Journal Phys. Chem. Ref. Data, Vol.2, pp. 757-922, 1973

(18) Wegener, P.P. and Mack, L.M.:
Condensation in supersonic and hypersonic wind tunnels. In: Advances in Applied Mechanics, Vol. V (edited by H.L. Dryden/Th. v. Kârmân et al).
Academic Press, New York, 1958

(19) Oswatitsch, K.:
Kondensationserscheinungen in Überschalldüsen. Zeitschrift für angewandte Mathematik und Mechanik, Vol. 22, pp. 1-14, 1942

(20) Wegener, P.P.:
Nonequilibrium flow with condensation.
Acta Mechanica, Vol. 21, pp. 65-91, 1975

(21) Green, J.E., Weeks, D.J., and Pugh, P.G.:
Heat transfer as a source of spurious scale effects in subsonic and transonic wind tunnels. In: Proc. First Int. Symp. on Cryogenic Wind Tunnels, Southampton, 1979

(22) Zierep, J.:
Theory of flows in compressible media with heat addition. AGARDograph No. 191, 1974

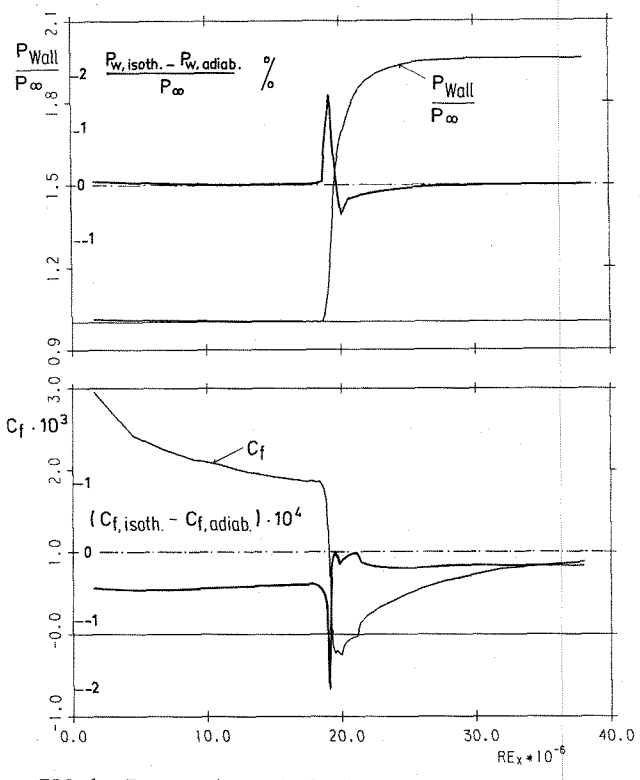

FIG.1: Transonic Normal Shock Wave-Turbulent Boundary Layer Interaction with Heat Transfer (Isothermal Wall)
$Re = 20 \cdot 10^6; M_\infty = 1.35; T_{Wall} = 1.1 \cdot T_{Recovery}$

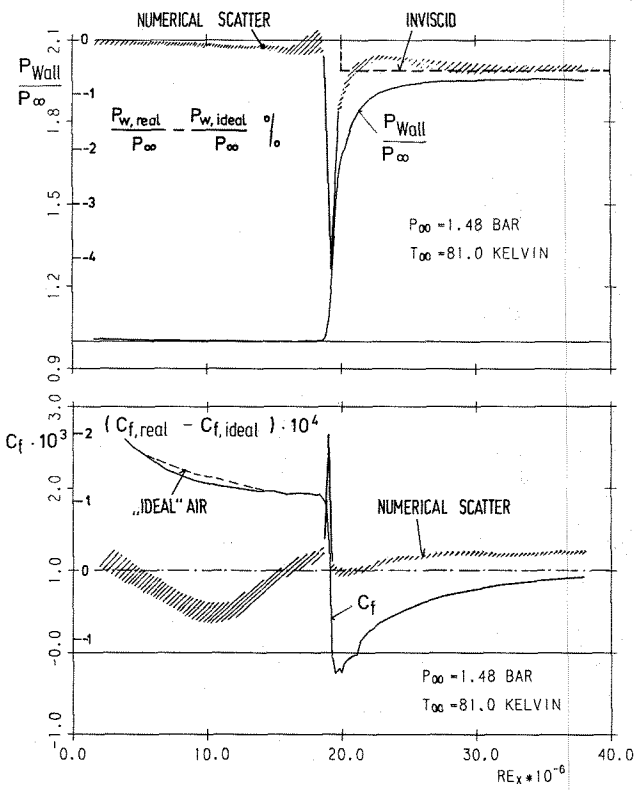

FIG.2: Transonic Normal Shock Wave-Turbulent Boundary Layer Interaction in Real Nitrogen Close to Saturation.
$Re = 20 \cdot 10^6; M_\infty = 1.35$; Adiabatic Wall

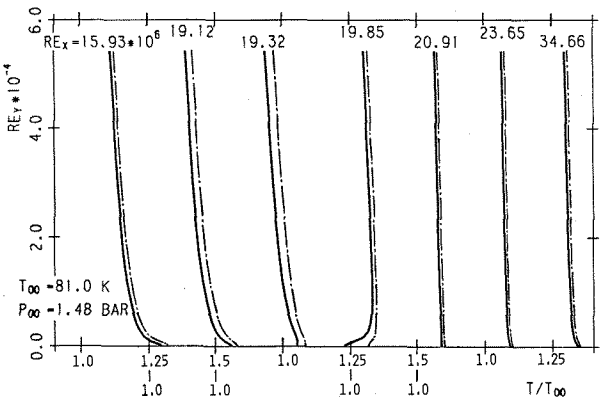

FIG.3: Transonic Normal Shock Wave-Turbulent Boundary Layer Interaction
- Comparison of Adiabatic Temperature Profiles in Real Nitrogen and "Ideal" Air
—— Real Nitrogen; •—•—• "Ideal" Air

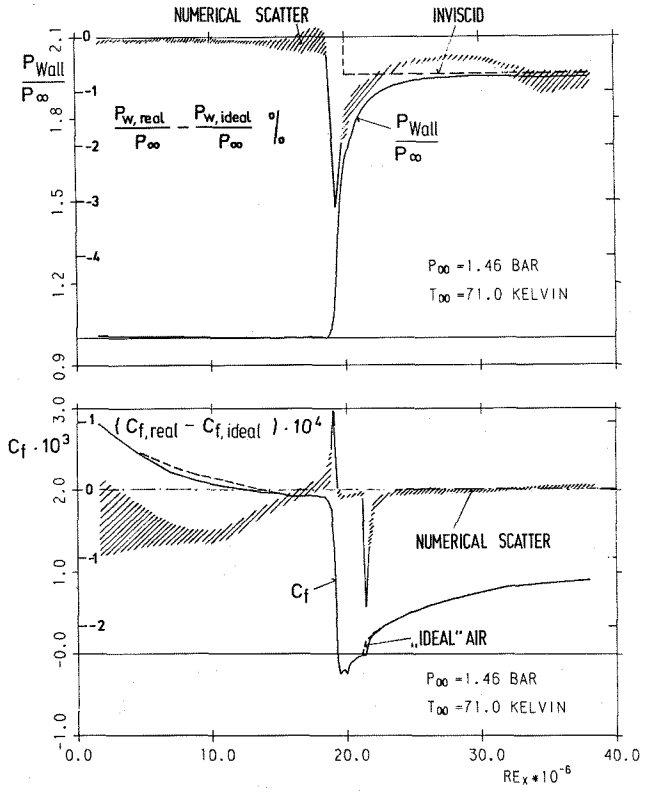

FIG.4: Transonic Normal Shock Wave-Turbulent Boundary Layer Interaction in Supersaturated Real Nitrogen
Re=20•10^6; M_∞=1.35; Adiabatic Wall

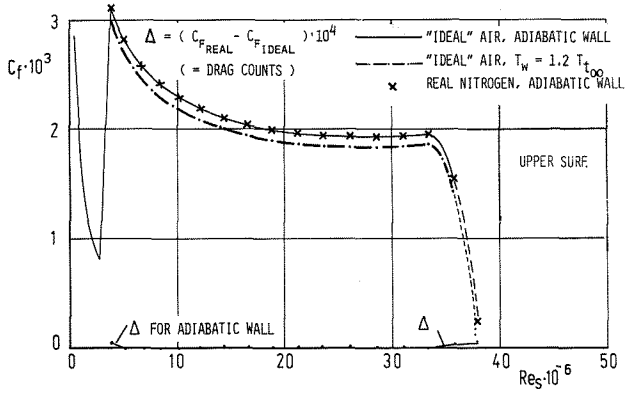

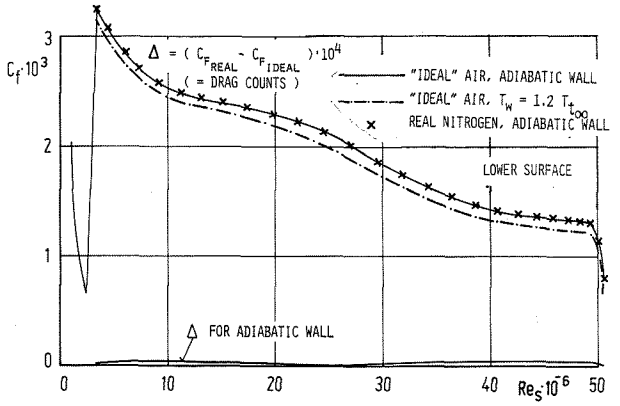

FIG.5: Boundary Layer Calculations for Airfoil Section Dornier A2 (CAST 10) in Transonic Flow
Re = 50•10^6; M_∞ = 0.76; α = 5°
"Ideal" Air : T_{t_∞} =245 K
Real Nitrogen: p_{t_∞} =4.5 bar; T_{t_∞} =110 K

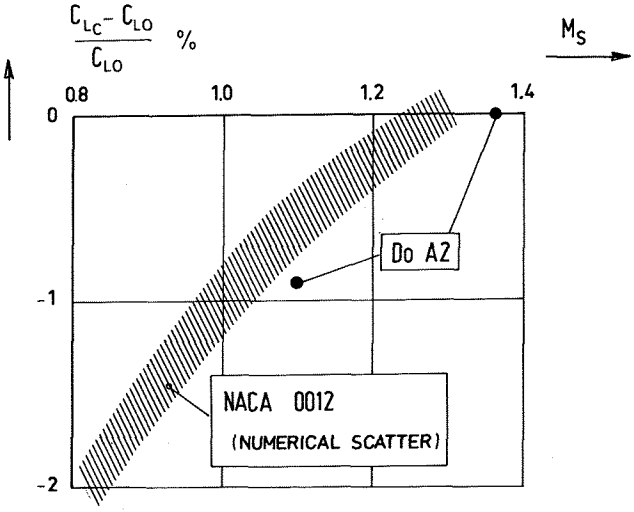

FIG.8: Lift Reduction by Condensation

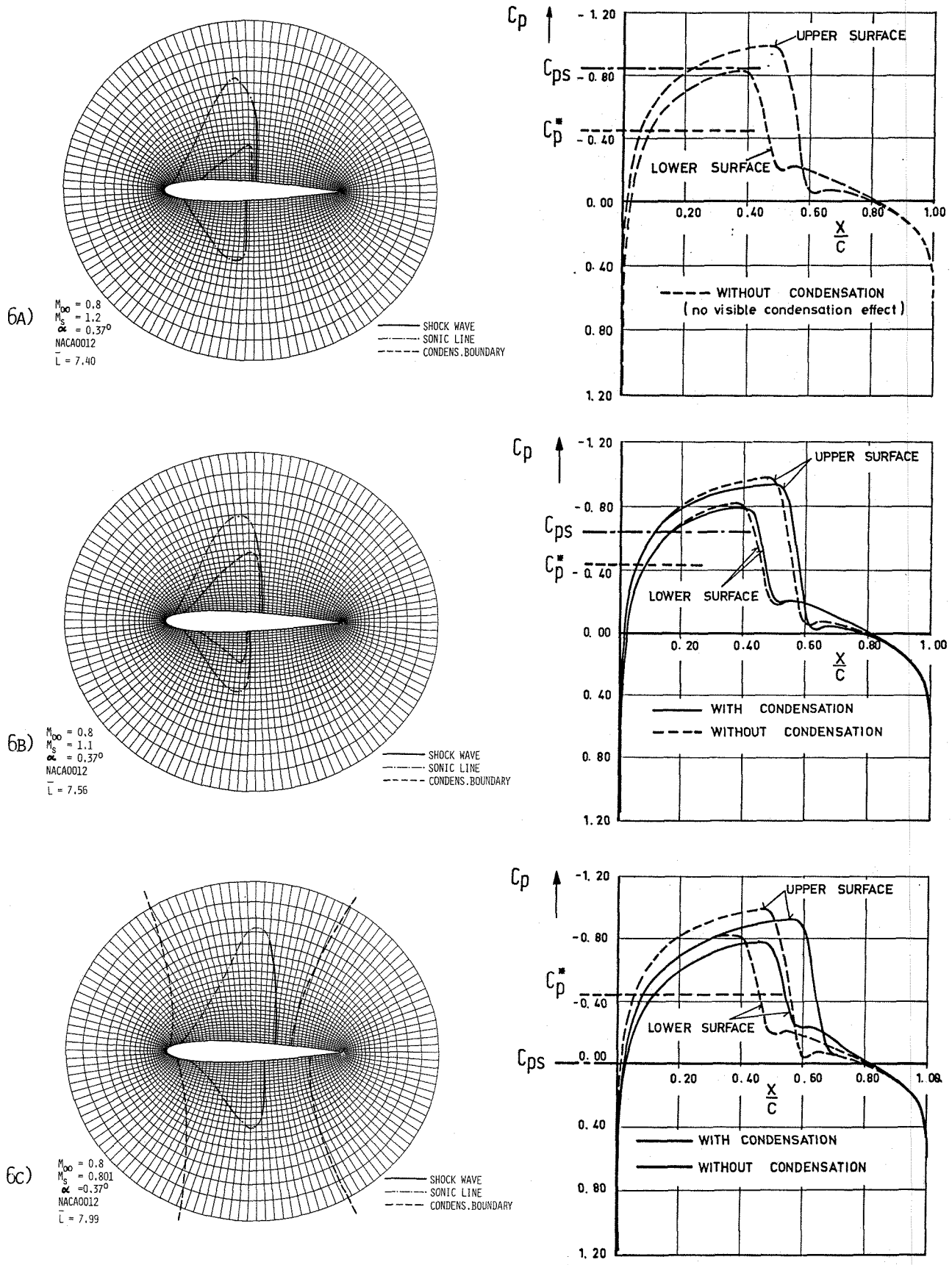

FIG.6: Computational Mesh, Supersonic Regions, Condensation Zones, and Pressure Distributions for Airfoil Section NACA 0012; M_∞ = 0.8 ; α = 0.37°; Different Saturation Mach Numbers

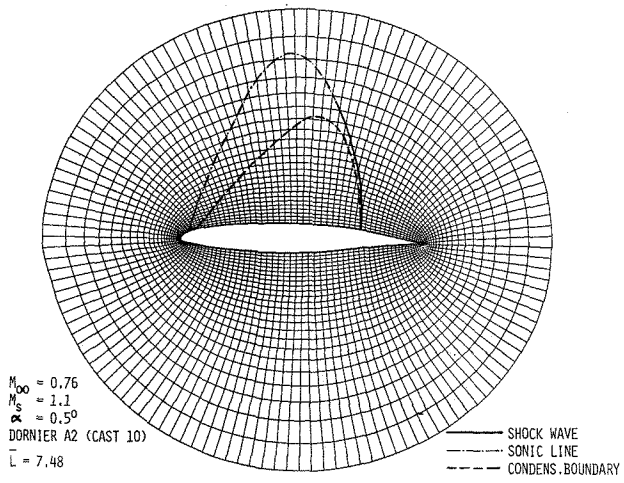

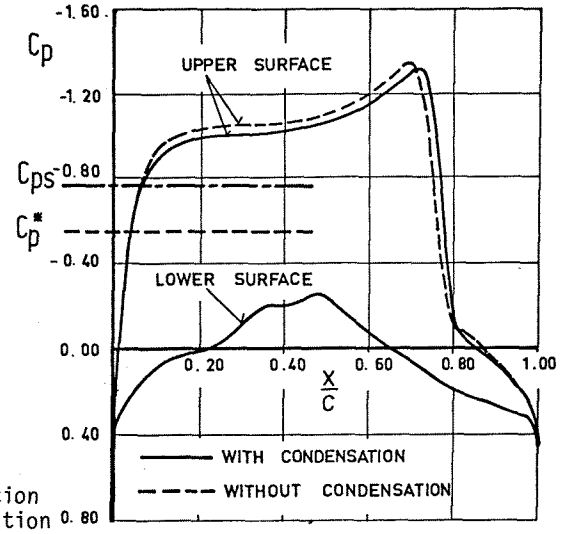

FIG.7: Computational Mesh, Supersonic Region, Condensation Zone, and Pressure Distributions for Airfoil Section Dornier A2 (CAST 10) ; $M_\infty = 0.76$; $\alpha = 0.5^0$; $M_s = 1.1$

FIG.10: Condensed Mass Fraction on Different Airfoil Surface Streamlines

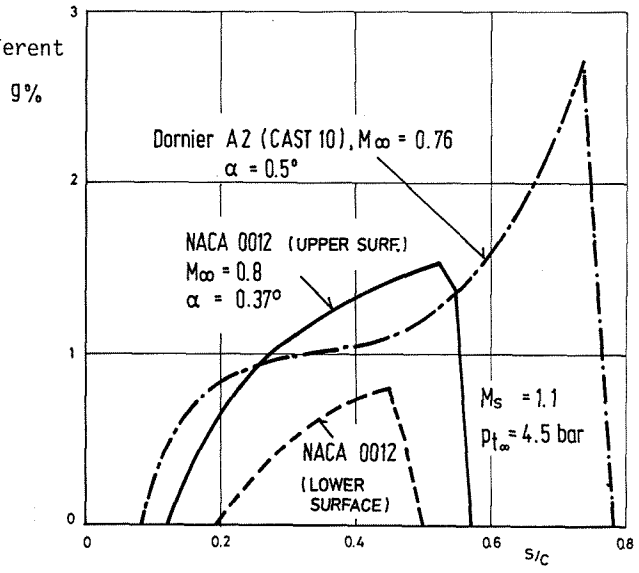

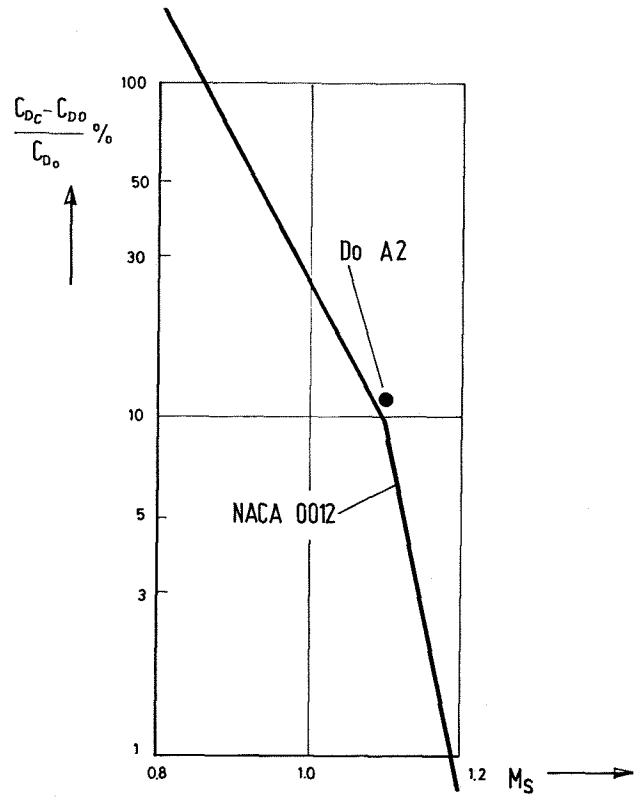

FIG.9: Drag Rise by Condensation

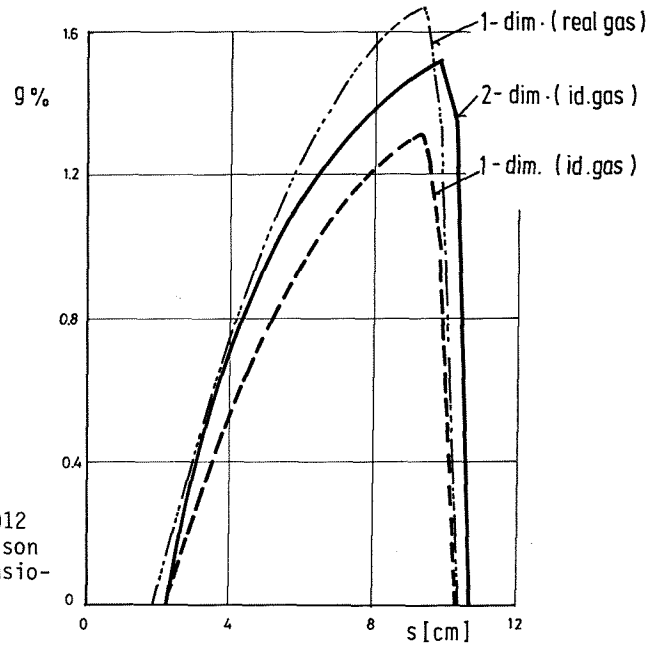

FIG.11: Condensed Mass Fraction on NACA 0012 Upper Surface Streamline - Comparison between Two-Dimensional, One-Dimensional, and One-Dimensional Real Gas Solution